

B. BIAŁOBRZESKA^{1*}, R. DZIURKA²

EFFECT OF BORON ACCOMPANIED BY CHROMIUM, VANADIUM AND TITANIUM ON THE TRANSFORMATION TEMPERATURES OF LOW-ALLOY CAST STEELS

The purpose of the research was to examine the influence of boron on the selected properties of low-alloy cast steels. The chemical compositions of the cast steels were designed especially for this study to contain different alloy elements. The first composition lacked significant alloying elements. The subsequent grades of cast steels had the addition of chrome, chrome with vanadium, and chrome with titanium. It was decided to investigate the influence of boron in the presence of such alloying additives on the temperature of phase transformations. On the basis of dilatometric curves, the characteristic temperatures of the phase transformations were determined. Additionally, to assess the influence of the cooling rate on the structure of cast steels, an analysis of their microstructure, after full annealing and quenching, was carried out.

Keywords: boron; cast steels; dilatometric research; microstructure

1. Introduction

As per the ISO 3755:1991 standard, non-alloy cast steels contain 1% of alloy additions, low-alloy cast steels contain up to 2.5% of alloy additions, and medium-alloy ones contain between 2.5 and 5% of alloy additions, with cast steel being classified as a high-alloy one if the alloy content exceeds 5% [1]. Particular attention should be paid to the group of low-alloy cast steels known as micro-alloyed steels. These steels contain certain amounts of 'basic' alloy elements, with the concentration of which often even exceeding 1% (usually they are used for the purpose of reducing and deoxidising steel). According to the classical division, they are defined as medium-alloy cast steels, however, their special properties are due to dopants in quantities of a hundredth or a thousandth part of a percentage point. The clear influence of micro-additions can usually be observed after properly conducted heat treatment, which means that the structure is strengthened by the release of fine dispersion phases, which in turn improve the hardness, strength, and tribological properties of the material. The most frequently used additions are rare earth elements, or elements that make hard, high-melting phases, such as Ti, B, V, or Nb [2-5].

Among these elements, boron deserves special attention. It increases the hardenability of steel, even when the amount of

this element would be considered to be "trace" in the case of other elements. The strongest influence of boron is observed when its content is higher than 0.0005-0.0008%, yet at the same time not exceeding 0.003-0.005%. However, its influence strongly depends on the carbon content in the steel, and decreases when the carbon content increases. When the carbon content reaches the value of about 0.8%, it nearly completely disappears [6,7]. This strong influence of boron results from its very low solubility in ferrite and austenite. However, due to the high diffusion rate, boron accumulates in the marginal areas of grains and in other defects, which hampers the creation of embryos and, consequently, delays diffusion transformations. Boron must be used, together with other special alloy additions, in a complex way, otherwise its effect is limited. It is assumed that the effect of boron is related to both its high affinity for nitrogen and the creation of boron nitrides BN, which thus limits the amount of boron dissolved in solution. The difficulty in preventing boron from bonding to nitrides, as well as the fact that an excessively high boron content not only hinders the improvement in hardenability, but also promotes brittleness through the formation of compounds with iron, means that this element is only marginally used as an alloying element. It was only the accidental use in 1935 of a ferroalloy as a deoxidiser (which also contained elements that protected boron from binding with oxygen

¹ WROCLAW UNIVERSITY OF SCIENCE AND TECHNOLOGY, DEPARTMENT OF VEHICLE ENGINEERING, SMOLUCHOWSKIEGO STR. 25, 50-370 WROCLAW, POLAND

² AGH UNIVERSITY OF SCIENCE AND TECHNOLOGY, FACULTY OF METALS ENGINEERING AND INDUSTRIAL COMPUTER SCIENCES, AL. A. MICKIEWICZA 30, 30-059 KRAKOW, POLAND

* Corresponding author: Beata.bialobrzaska@pwr.edu.pl



and nitrogen) in the metallurgical process that made it possible to appreciate boron as an alloying additive for improving hardenability. Since then there have been significant advances in materials engineering towards the development and production of steels with boron. Today's boron steels, known as low-alloy boron steels, martensitic boron steels or wear-resistant boron steels, are produced by a number of metallurgical companies [8].

These steels, due to the high abrasion resistance declared by their manufacturers, as well as their satisfactory and often high impact strength, have been the subject of numerous studies. Since boron is an element that promotes the growth of austenite grains and lowers the temperature of the beginning of grain growth, the authors focused on a comparative analysis of the prior austenite grain size of various types of wear-resistant steels austenitized at different temperatures and times [9]. In addition, the effect of the austenitizing temperature, and thus the prior austenite grain size on a number of properties was investigated. For example, the authors analysed the influence of the grain size of Hardox 450 on the phase transformations of undercooled austenite occurring during continuous cooling [10]. It was observed that an increase in the austenitizing temperature caused a shift in the bainitic transformation and diffusion transformations towards longer times, which makes it possible to obtain a bainitic structure, even during continuous cooling. The influence of the austenitizing temperature, and thus the austenite grain size, on the utilitarian properties of Hardox 450 steel, such as abrasive wear resistance, impact strength, tensile strength, elongation, and constriction at break was also analysed [11,12]. However, most such studies concern the tribological properties of wear-resistant boron steels [13-20]. The most recent research, however, concerns technological properties, such as weldability, as well as attempts to recover the structure and thus the mechanical properties degraded by high-temperature thermal processes during the joining of sheets [21-24].

The above studies concern the properties that were tested on commercial steel grades. In principle, they made it impossible, apart from in comparative analyses of various steel grades, to interfere with their chemical composition. In each of these grades, in addition to elements such as e.g. chromium, titanium and vanadium, the boron was an alloying additive, which made it difficult to assess the pure influence of this element on a number of mechanical properties. Therefore, it was decided to design cast steel with such a chemical composition that would allow the effect of boron itself to be assessed, as well as the effect of boron in the presence of chromium, or chromium and vanadium, or chromium and titanium on the structural and mechanical properties to be examined. They also allowed a certain utilitarian aspect to be achieved, because in the course of the research it turned out that the designed cast steel with a complex addition of boron, chromium and vanadium can be successfully used as a material that has satisfactory abrasion resistance [25]. It should also be added that owing to the elimination of forming, the manufacturing process of cast steels is cost-effective, which in times of economic crisis increases the application spectrum of this material. Shaping the material in casting forms results in

considerable savings [1,26,27], and the deliberate introduction of suitable elements into the cast steel makes it possible to improve selected properties, such as hardenability, impact toughness, and hardness when compared to non-alloyed cast steels.

The varying chemical compositions of the investigated melts provide the basis for interesting comparative results. The ingots will therefore be the subject of the tests, to which some commercial grades of wear-resistant steels were previously subjected to. To date, the effect of boron in the presence of chromium, vanadium and titanium on the austenite grain size [28], and also its effect on hardenability on the basis of the Jominy test [29] has been analysed. However, the mentioned alloying elements, which are dissolved in an iron solid solution and introduced in appropriate amounts, influence the position of the critical points in the iron-cementite diagram. This means that alloy additions can appropriately decrease or increase the temperature of phase transformations in materials. Moreover, they can shift the occurrence of such transformations to places with a lower or higher carbon content in an alloy [30,31]. In the case of carbon cast steels, in which the participation of these elements is small, the shift of points does not generally occur. In alloy cast steels, these changes may be very clear, and the awareness of their occurrence is significant with respect to designing the chemical composition and suitable heat treatment. Alloy elements, which dissolve in both ferrite and carbides, can also shift the points of mixtures, such as perlite and ledeburite, to lower carbon content in cast steels. The reduced carbon content in a eutectoid mixture indicates the possibility of the disappearance of ferrite in the microstructure at either lower carbon contents or in the presence of more carbides outside the eutectoid [30]. Of particular interest is the influence of boron on the kinetics of the transformation of undercooled austenite, especially with regards to other alloying elements. However, this influence is complex, and the results of many studies can be seen to be contradictory. From a utilitarian point of view, the most important is the effect of boron on the incubation period of the austenite-ferrite transformation. This element reduces the rate of the nucleation and grain growth of polygonal ferrite, and increases the incubation period of the transformation [32-34]. A decrease in the boundary energy of austenite grains will inhibit the nucleation of ferrite at these locations. As a result, the austenite will either be stable at a lower temperature, or it will transform into martensite or bainite (depending on the chemical composition and cooling rate) instead of ferrite [35]. However, experimental results concerning changes in the position of the austenite minimum stability temperature in boron steels are not unambiguous. Some data show an increase in the minimum austenite stability temperature [36], while others show a decrease [37]. Since the effect of alloy additions may be hard to predict or calculate, data usually present the influence of individual elements on the position of both the critical temperatures of phase changes and the points in the iron-cementite diagram. Therefore, the authors' interest lies in the complex analysis of the influence of boron on the temperature of phase transformations of low-alloy cast steels when boron is the only alloy element, or when, apart

from boron being the main alloy element, there are also chromium, chromium and vanadium, and chromium and titanium.

2. Material and methods

The research material consisted of 8 melts of various chemical composition. The casting moulds were made of bentonite mass using wooden models of an earlier agreed shape. The smelting cast steel of a specified chemical composition was conducted in an average frequency induction oven – Radyne type, 100 kW, 120 kg capacity, and with a neutral lining. Each fed batch was about 110kg. Above the crucible, a special type of hood was mounted so that argon could be blown underneath for the purpose of maintaining the complex chemical composition. The batches that were used for smelting were composed of: ARMCO iron, low-carbon steel scrap, and Fe Mn 80, FeCr 60, Mn and carburizer additions. Depending on the selected chemical composition, the following were also added: FeB 8, FeTi 25, FeV 70, Al, Ti. After melting a batch and conducting temperature measurements, a sample was taken to determine the chemical composition. If necessary, the composition was supplemented, and then, before pouring the content into a mould, additions that could be burned out were made. Melted metal was poured into a previously heated ladle, the temperature was measured, and a sample was taken to determine the final chemical composition. The pouring temperature was 1540°C. After chilling and cleaning the mould to eliminate the remnants of the mass, the flash was removed.

The chemical composition of the ingots was analysed using an optical spectrometer ARL NA using spark excitation. This was not the case for the content of boron and other elements occurring in minimum amounts, which were instead determined using the nuclear spectroscopy absorption method with Solaar M6 Thermo equipment, or the spectral method with the application of a Leco Glow Discharge Spectrometer GDS-500A. The used melts allowed the influence and efficiency of the single or complex introduction of micro-additions, differing in terms of the content of such elements as boron, chromium, vanadium and titanium, to be tested. A boron content exceeding the alloy limit value was found in melts 1, 3, 5 and 7; a chromium content exceeding the alloy limit value was found in melts 3, 4, 5, 6, 7 and 8; a vanadium content exceeding the alloy limit value was found in melts 5 and 6; and a titanium content exceeding the alloy limit value was found in melt 8 (TABLE 1).

Samples were taken from the ingots and completely annealed at a temperature of 1200°C. They then underwent normalising at a temperature of 900°C for one hour, and quenching in water at a temperature of 1200°C. The heat treatment was conducted in a protective argon atmosphere in a FCF 12 SHM/R conventional gas tight retort furnace.

Dilatometric tests were made using a Linseis L78 RITA dilatometer on $\varnothing 3 \times 10$ mm samples. During the tests, the characteristic temperatures of the transformations were determined. The dilatometric method is an essential test for determining the basic data used in heat treatment. The principle of dilatometric

TABLE 1

Chemical composition of the analysed melts

No of melts	C [%wt]	Mn [%wt]	Cr [%wt]	V [%wt]	Ti [%wt]	B [%wt]
1	0.31	0.30	0.027	0.002	0.002	0.002
2	0.34	0.59	0.030	0.006	0.002	—
3	0.41	1.32	0.900	0.010	0.005	0.003
4	0.36	1.34	0.850	0.009	0.004	—
5	0.38	1.37	0.990	0.260	0.006	0.003
6	0.37	1.40	0.970	0.275	0.013	—
7	0.38	1.40	0.900	0.010	0.019	0.003
8	0.30	1.45	1.000	0.013	0.059	—

Si at a similar level of 0.34÷0.47, P at a similar level of 0.016÷0.018, S at a similar level of 0.009÷0.011, Ni at a similar level of 0.044÷0.112, Mo at a similar level of 0.013÷0.030, Cu at a similar level of 0.043÷0.110, Al at a similar level of 0.022÷0.039.

research is very simple, but it is thanks to this that it is possible to precisely determine many important parameters of virtually any material. In the case of metallic materials, and in particular new alloys, changes in the coefficient of thermal expansion with temperature, the critical temperatures of phase transformations, and phase transformations during cooling are determined. Based on these data, the parameters of heat treatment, i.e. annealing, hardening and subsequent tempering, can be designed. In this study, a heating and cooling curve was performed according to the scheme and parameters shown in Fig. 1a. Two sets of diagrams, heating (1b) and cooling (1c), were made from the obtained results. Each diagram consists of two curves, i.e. the dilatometric curve (blue – ΔL), which shows the changes in the length of the sample with temperature, and the second curve, which shows the changes in the coefficient of thermal expansion with temperature ($TEC\alpha$). The TEC coefficient was calculated according to formula (1).

$$TEC\alpha = \frac{\Delta L}{L_0 \cdot \Delta T} \quad (1)$$

An analysis of each set of diagrams for each melt was performed. For better clarity, it was decided to compile only a part of the results. Only the curves of the changes in the coefficient of thermal expansion are listed in the further part of the article. In the case of TEC (due to the fact that it is absolute), often occurring subtle changes are the best to observe, and therefore two materials are the easiest to compare.

Additionally, it was decided to compare the obtained results with the calculated temperatures. In the available literature, only the following formula for the Ac_3 temperature was found [38], which takes into account all the elements present in the melts, in particular the addition of boron:

$$\begin{aligned} Ac_3 = & 912 - 370C - 27.4Mn + 27.3Si - 6.35Cr \\ & - 32.7Ni + 95.2V + 190Ti + 72Al + 332S + 276P \\ & + 485N - 900B + 16.2CMn + 32.3CSi + 15.4CCr \\ & + 48CNi + 4.32SiCr - 17.3SiMo - 18.6SiMo - 18.6SiNi \\ & + 4.8MnNi + 40.5MoV + 174C^2 + 2.46Mn^2 - 6.86Si^2 \\ & + 0.322Cr^2 + 9.96Mo^2 + 1.24Ni^2 - 60.2V^2 \quad (2) \end{aligned}$$

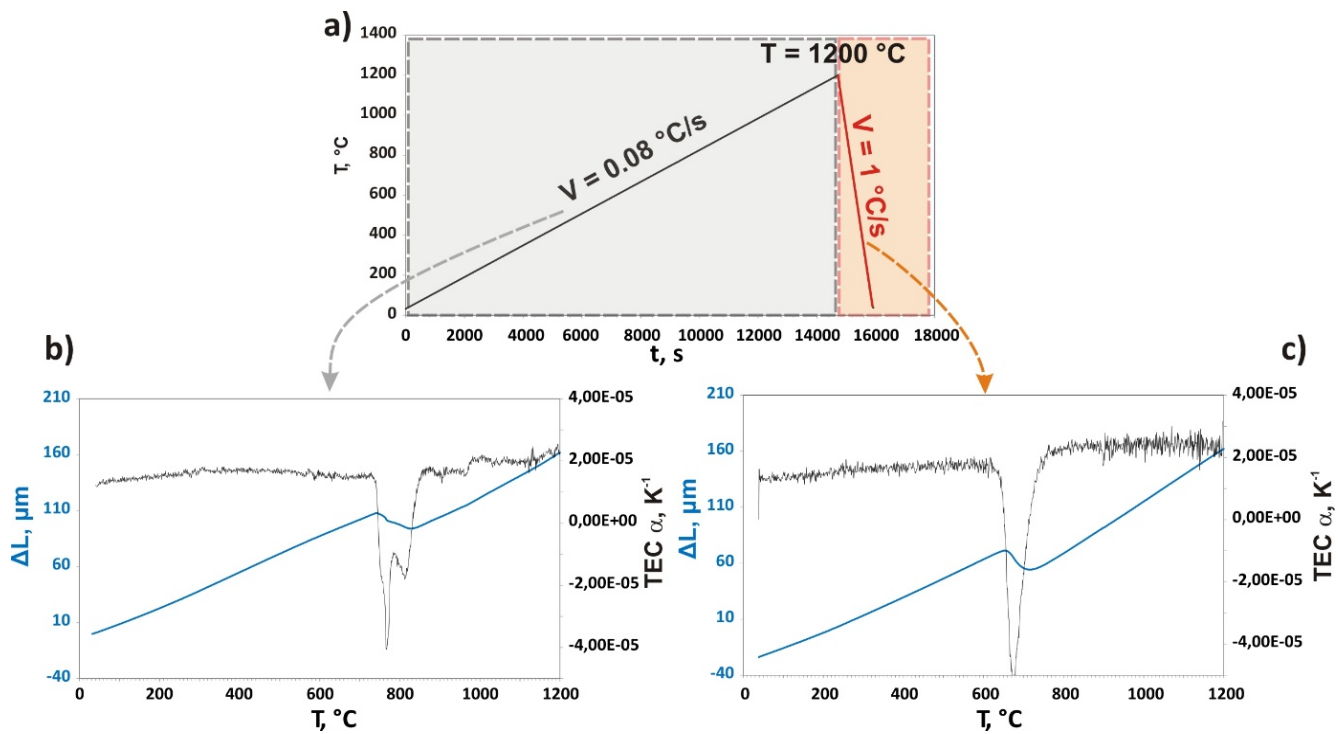


Fig. 1. Results of dilatometric tests: a) test parameters, b) dilatometric curve of heating (ΔL) with a corresponding curve of thermal expansion coefficient ($TEC\alpha$), and c) dilatometric curve of cooling with a corresponding curve of changes of the thermal expansion coefficient

For the observation of the structures, a Nikon ECLIPSE MA200 was used. The structures were etched using reagent 74 (5% HNO_3 solution in alcohol) acc. to ASTM E407. Moreover, hardness measurements were also conducted using static Brinell tests as per the EN ISO 6506-1:2014 standard. For this purpose, a Zwick/Roell ZHU testing machine, a ball with a diameter of 2.5 mm diameter, and a load of 187.5 kg applied for 15s were used.

3. Results and Discussion

3.1. Dilatometric analysis

The results for the melts without boron are summarised in Fig. 2, and for the melts with boron in Fig. 3. The diagrams are divided into temperature ranges to make the observed changes clear. Three temperature ranges were analysed in detail for each set of curves. The first temperature range, from $31\div 650^\circ C$ (Figs. 2b and 3b), shows the transformations taking place just before the formation of austenite. The next temperature range ($650\div 950^\circ C$) covered the entire range of the austenite formation (Figs. 2c and 3c). The last temperature range is $950\div 1200^\circ C$ (Figs. 2d and 3d). In each figure, significant effects related to the phase transformations are marked with triangles. In the first heating range, two negative effects and one positive effect can be identified, which are related to the phase transformations. This means that the cast steels hardened, and we can observe the effects of the tempering of the material. The negative effect observed for melts 1, 3, 5 and 7 in the temperature range

of $260\div 440^\circ C$ is related to the precipitation of cementite. In the case of the melts without the addition of boron, the visible effects are weaker and occur only for melts 6 and 8. In this series of melts, negative effects are observed for melts 2 and 4 at temperatures much higher than $510^\circ C$. This is probably due to recrystallization. On the other hand, the observed positive effects come from the transformation of the residual austenite. Positive effects are only visible in the case of melts 5, 6, 7 and 8. The occurrence and transformation of the residual austenite was not influenced by boron, but only by the background of the remaining elements. As can be seen, it is only the interaction of chromium with vanadium (melts 5 and 6), or chromium with titanium (melts 7 and 8) that causes the stabilization of this phase during the cooling, and its transformation during heating.

On the basis of the results from Figs 2b and 3b, the critical temperatures were determined.

TABLE 2

Temperatures ($^\circ C$) of the phase transformation of the analysed melts during heating

Temperatures [$^\circ C$]	Melt 1	Melt 2	Melt 3	Melt 4	Melt 5	Melt 6	Melt 7	Melt 8
Ac_{1s}	740	730	715	740	720	740	690	725
Ac_{1f}	785	785	740	760	765	770	720	775
Ac_3	840	820	780	790	790	820	760	840
Ac_3 calculated	827	816	794	802	819	824	798	824

The characteristic temperatures of the phase transformations are shown in TABLE 2. The reference in the analysis was melt 2, which did not contain any substantial alloy additions.

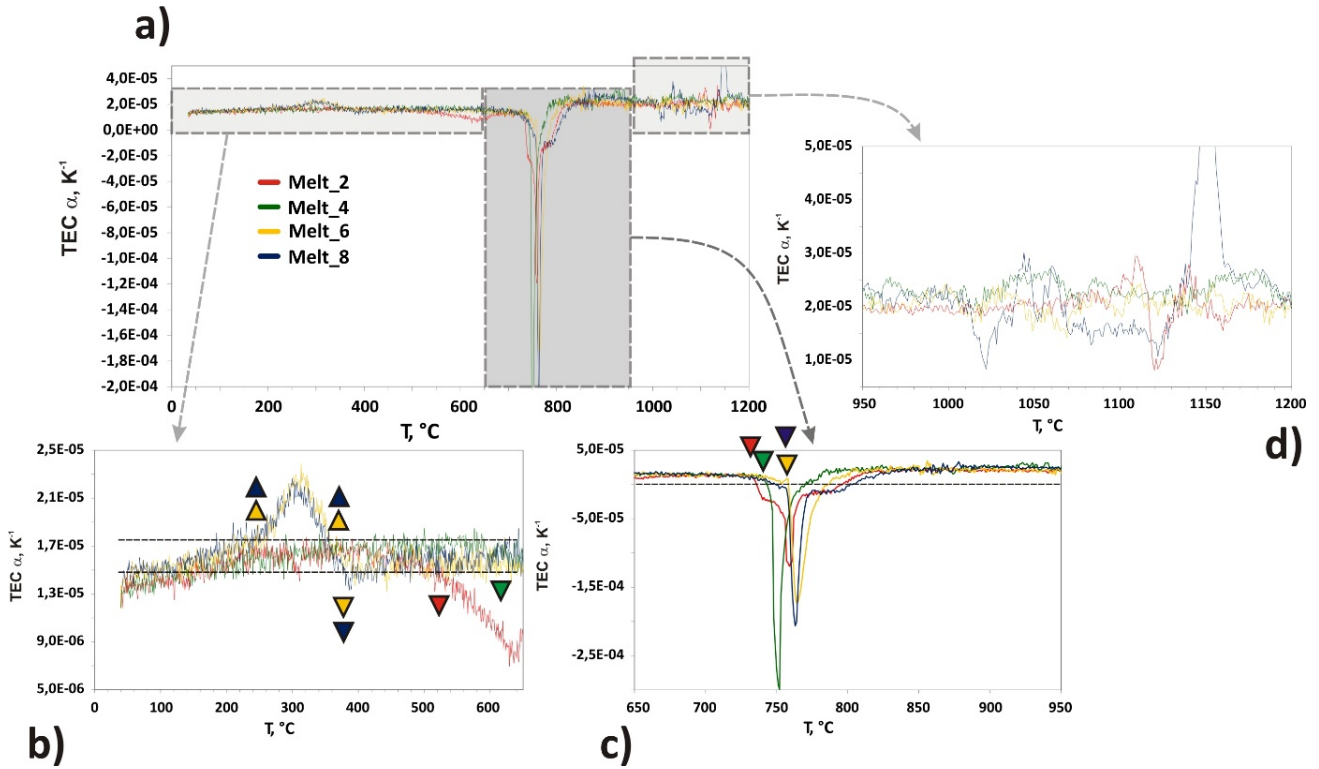


Fig. 2. Dilatometric curves with characteristic transformation temperatures of the analysed melts without the addition of boron

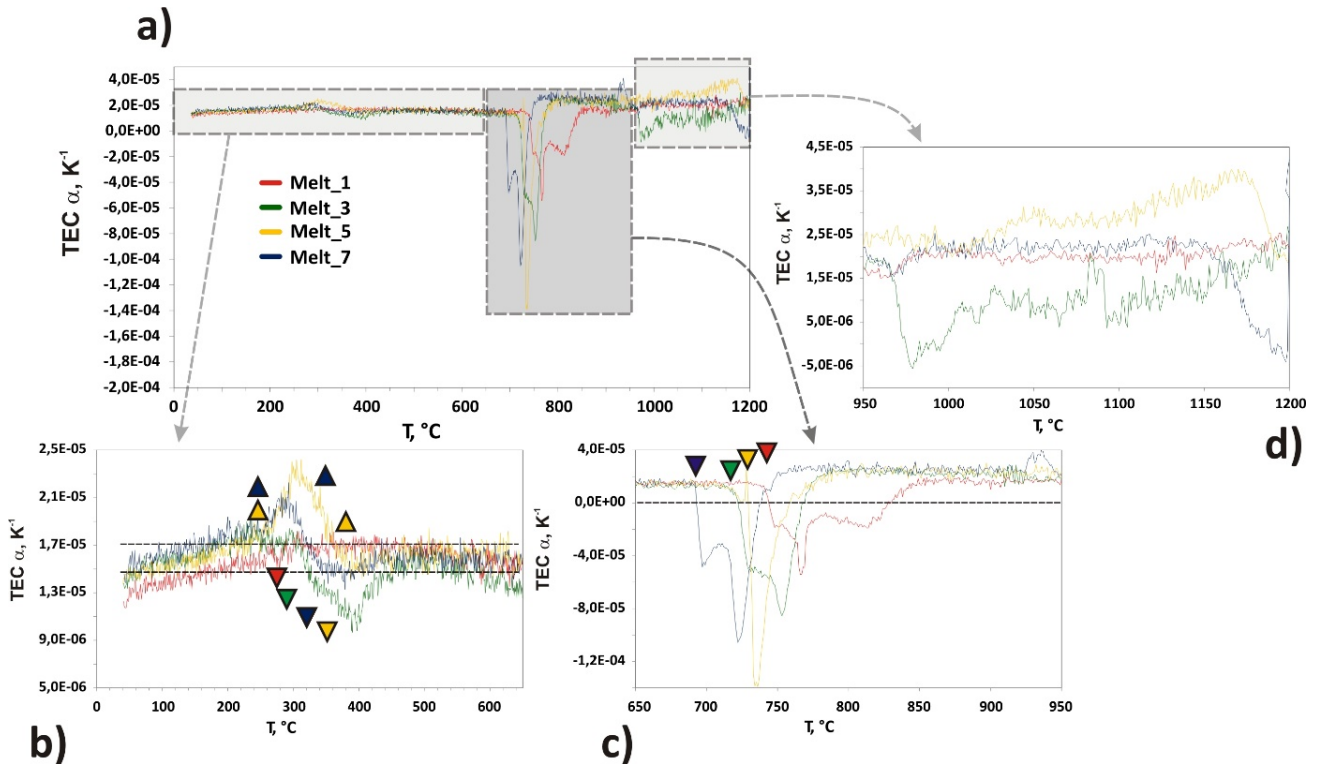


Fig. 3. Dilatometric curves with characteristic transformation temperatures of the analysed melts with the addition of boron

In the case of this melt, the transformation temperatures were $Ac_{1s} = 730^{\circ}\text{C}$, $Ac_{1f} = 785^{\circ}\text{C}$ and $Ac_3 = 820^{\circ}\text{C}$, respectively (TABLE 2 and Fig. 2). The temperatures of the phase transformations for melt 1 were $Ac_{1s} = 740^{\circ}\text{C}$, $Ac_{1f} = 785^{\circ}\text{C}$ and $Ac_3 = 840^{\circ}\text{C}$ (TABLE 2 and Fig. 3). Melt 1 contained 0.03%

more carbon than melt 2. This difference is too small to significantly affect the temperatures of the austenite formation, and therefore the increase in the temperature of the allotropic transformations was mainly due to the presence of boron. In the case of the melts containing chromium, i.e. 3 and 4, the ending

temperature of austenite forming was $-Ac_3 = 780$ and 790°C , respectively (TABLE 2, Figs. 2 and 3). The largest difference of 25°C was observed between the start temperatures of the perlitic transformation Ac_{1s} . Cast steels 5 and 6, containing chromium and vanadium, had a similar carbon content, which allowed its influence on transformation temperatures to be neglected. Despite this, when taking into consideration all the phase transformation temperatures, there were temperature differences of $15\text{--}30^\circ\text{C}$ between these melts (TABLE 2, Figs. 2 and 3). It is noteworthy that these temperatures were higher in the melt without the addition of boron. The difference in the carbon content between melts 7 and 8 was 0.08% , with such a difference possibly being responsible for a maximum change of 20°C between temperatures Ac_3 (TABLE 2, Figs. 2 and 3). In the case of the analysed melts, this difference was significantly higher and was equal to 80°C . Moreover, temperature Ac_3 , similarly to temperature Ac_{1s} , Ac_{1f} , was higher in the melt without boron.

The determined temperatures are summarized in Fig. 4. Thanks to such a comparison, the above considerations can be followed in detail. What is most important is that the determined temperatures and the observed influence of boron are confirmed by the calculations of the Ac_3 temperature. Even very large differences in the determined and calculated values can often be seen. Such differences may be caused by not taking into account all the elements present in the melt compositions. Additionally, as is the case in the calculations, the formula assumes that the entire element has an effect on temperature, and if carbide-forming elements (Cr, V, Ti) produce carbides, their influence is limited to only the part that is dissolved in the solution. However, the relationships determined from the dilatometric tests, as well as those calculated, are identical.

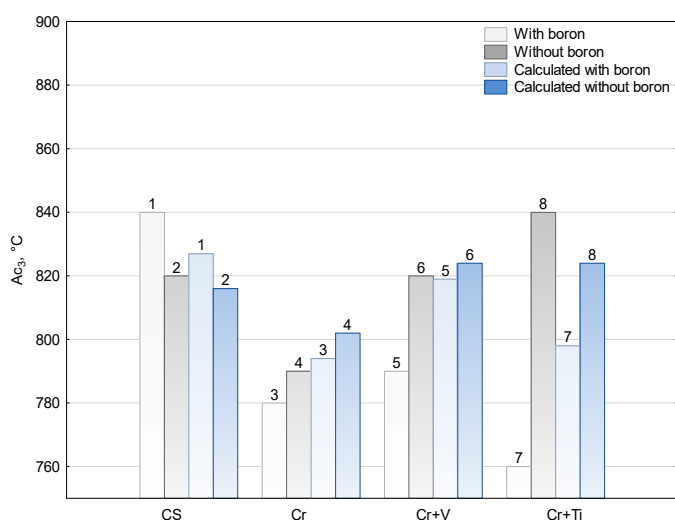


Fig. 4. Temperatures ($^\circ\text{C}$) of the phase transformation of the analysed melts during heating

The analysis of the dilatometric curves allowed for the conclusion that boron caused a small increase in the allotropic transformation temperature when it was not accompanied by any other alloy additions. The presence of chromium practi-

cally eliminated the influence of boron on the transformation temperatures, while in the presence of chromium and other micro-additions, such as vanadium and titanium, a decrease in all the phase transformation temperatures in the melts containing boron was recorded.

The next part of the article presents the results obtained during cooling (Fig. 5, TABLE 3). Due to the use of the same temperature and cooling rate, it is possible to make a conclusion regarding the influence of boron on the transformation of supercooled austenite. Additionally, the applied high temperature will dissolve most of the elements and enable a homogeneous solution to be obtained. Another positive effect of high temperature is the obtaining of a similar grain size of austenite, which has a significant impact on its transformation during cooling. In each of the studied cases, a significant influence of the addition of boron, as well as the background of other elements, can be seen. Even in the case of melts 1 and 2, where there are no other significant alloying additions, it can be seen (for melt 1) that the start and finish of the diffusion transformations were shifted to higher temperatures. This confirms the results described above. In the case of the subsequent melts, when there is a significant background of other elements, it can be seen that boron significantly increases the hardenability of the cast steels. In each case, the addition of boron decreased the temperature of the bainite and martensitic transformation. In the case of the pair of melts 5, 6 and 7, 8, the addition of boron shifted the diffusion transformations to longer times, with a bainitic-martensitic microstructure being obtained. An important next step in the case of investigating the effect of boron will be the preparation of TTT diagrams.

TABLE 3

Temperatures ($^\circ\text{C}$) of the phase transformation during cooling

	F/Ps	F/Pf	Bs	Bf	Ms
Melt 1	760	640	—	—	—
Melt 2	700	590	—	—	—
Melt 3	—	—	555	340	340
Melt 4	—	—	570	445	440
Melt 5	—	—	510	360	—
Melt 6	690	600	530	360	300
Melt 7	—	—	535	350	310
Melt 8	710	590	560	375	315

3.2. Microstructure analysis

The structural analysis in different heat treatment states (after full annealing at 1200°C and quenching from 1200°C) also showed significant differences between the melts, in turn revealing the influence of boron and other alloying additives on the morphology of the obtained structures.

After full annealing, the structure of the ferrite in melt 1 was clearly large-grained, and the ferrite showed a grain-like morphology (Fig. 6a). The hardness of melt 1 was 140 HBW (Fig. 14). In the case of cast steel 2, the structure was fragmented (Fig. 7a).

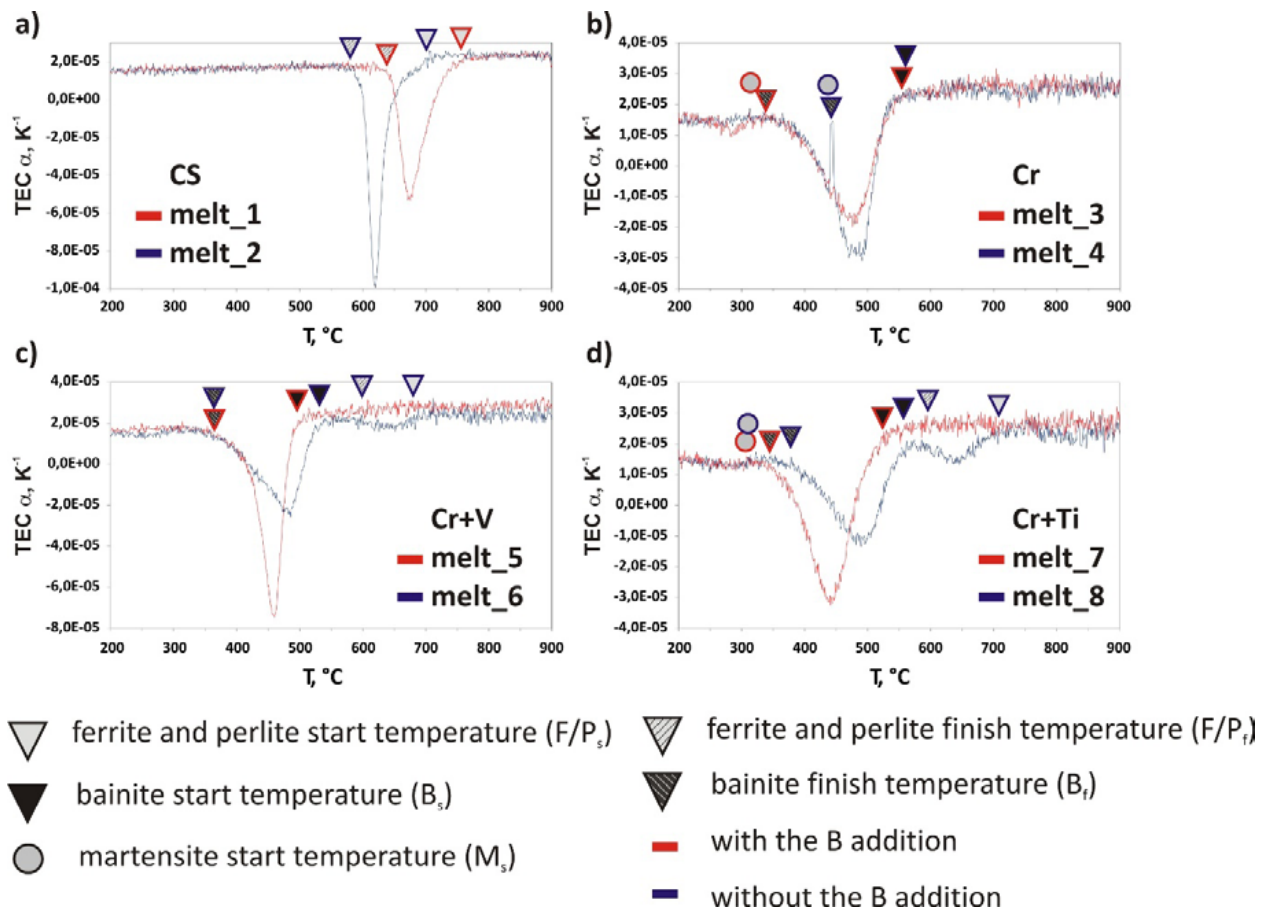


Fig. 5. Temperatures ($^{\circ}\text{C}$) of the phase transformation during cooling

In some places, the ferrite created a lattice around the perlite grains, and the alloy hardness was equal to 150 HBW (Fig. 14). In melts 3 and 4, ferrite was precipitated, which created a lattice at the quasi-perlite grain boundaries (Figs. 8a and 9a). However, in the case of the melt without boron, the lattice was thicker. The hardness of melts 3 and 4 was 243 and 213 HBW, respectively (Fig. 14). In the melts containing vanadium, i.e. 5 and 6, the ferrite was also precipitated after full annealing; it formed a thick lattice around the quasi-perlite, and also took a grain-like form while making ferritic zones in the structure (Figs. 10a and 11a).

The hardness of cast steel 5 was 215 HBW, while for cast steel 6 it was 237 HB (Fig. 14). Similar structural transformations were observed in melts 7 and 8 (Figs. 12a and 13a). However, in comparison with the melt containing boron, the ferrite precipitates in cast steel 8 covered a larger area in the structure, creating both a lattice and clusters of grain-like precipitates. The melt hardness was 209 HBW (Fig. 14). In melt 7, quasi-perlite covered a significantly larger area, while ferrite was precipitated at the grain boundaries, but it did not form a continuous envelope. The hardness of the boron melt was 236 HBW (Fig. 14).

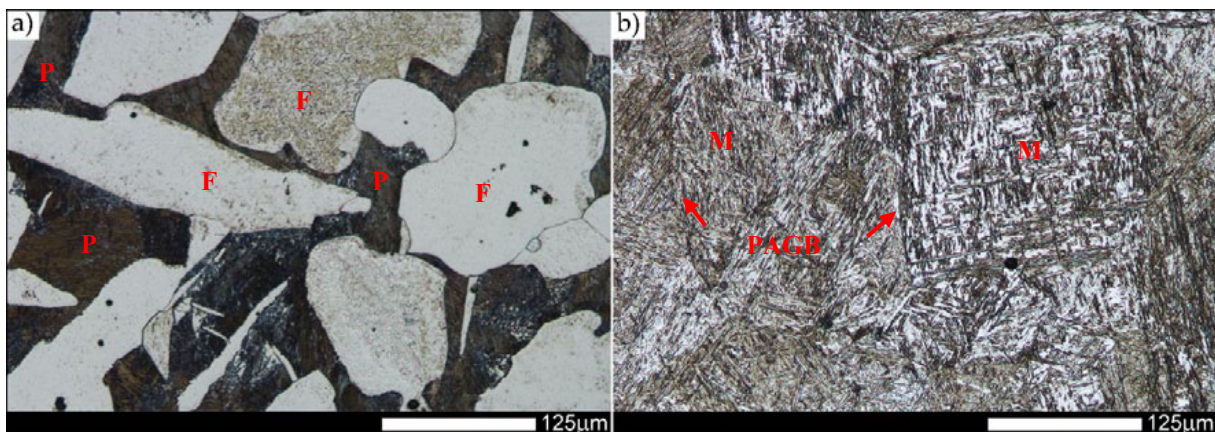


Fig. 6. Microstructures of melt 1 in different states of heat treatment: a) after full annealing; b) after quenching. Etched state, light microscopy. F – ferrite, P – perlite, M – martensite, PAGB – prior austenite grain boundary marked with arrows

In the case of the alloys containing chromium, vanadium, and titanium, the boron limited ferrite participation after full annealing. Moreover, the presence of alloy additions successfully limited the influence of boron on the development of large grains in the structure.

In the structure of melt 1, which was characterised by a coarse-grained structure, a large amount of untransformed aus-

tenite was visible against the background of martensite needles after quenching (Fig. 6b). This resulted in a hardness value of 516 HBW (Fig. 14). The martensite in melt 2 was also coarse-grained (Fig. 7b), but it was possible to observe acicular ferrite on the prior austenite grain boundary. Between the martensite, as in the case of melt 1, untransformed austenite was visible. The hardness of melt 2 was 560 HBW (Fig. 14).

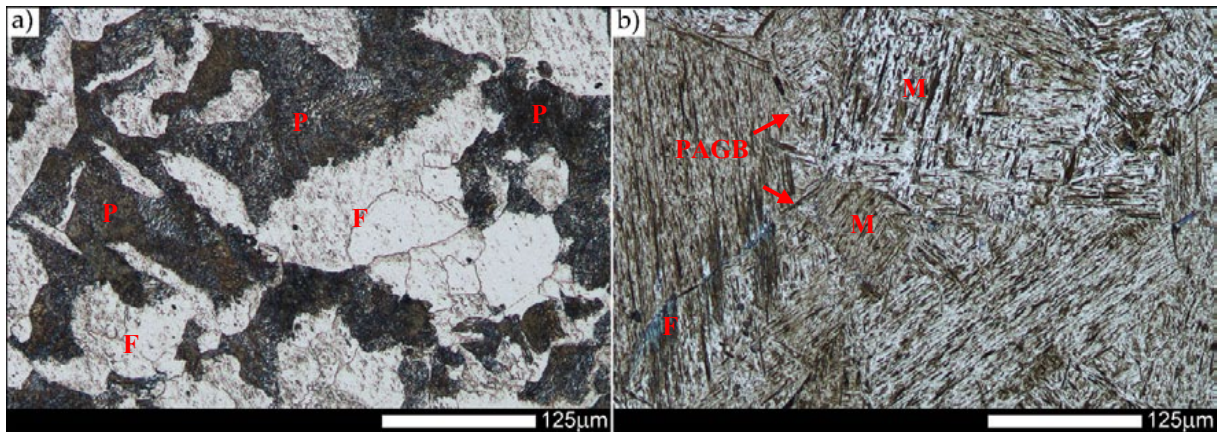


Fig. 7. Microstructures of melt 2 in different states of heat treatment: a) after full annealing; b) after quenching. Etched state, light microscopy. F – ferrite, P – perlite, M – martensite, PAGB – prior austenite grain boundary marked with arrows

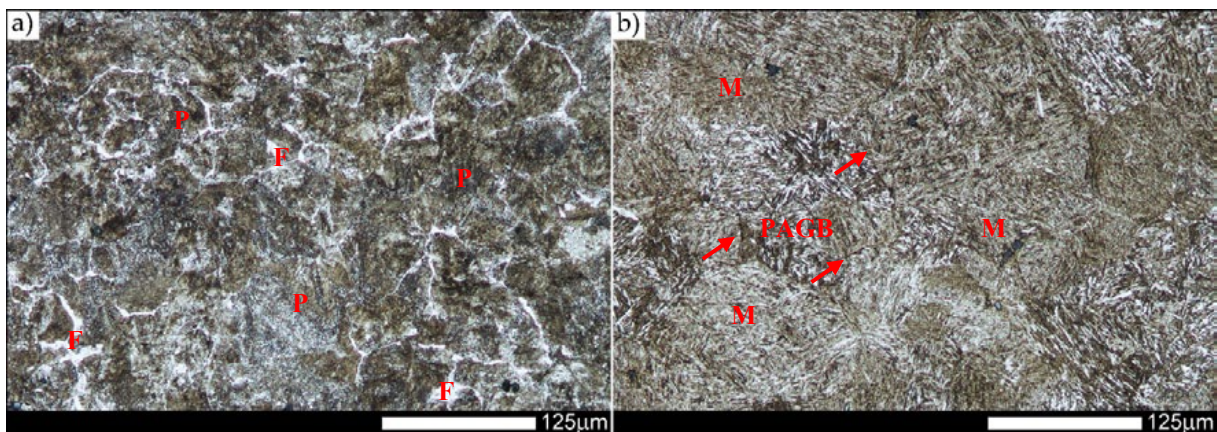


Fig. 8. Microstructures of melt 3 in different states of heat treatment: a) after full annealing; b) after quenching. Etched state, light microscopy. F – ferrite, P – perlite, M – martensite, PAGB – prior austenite grain boundary marked with arrows

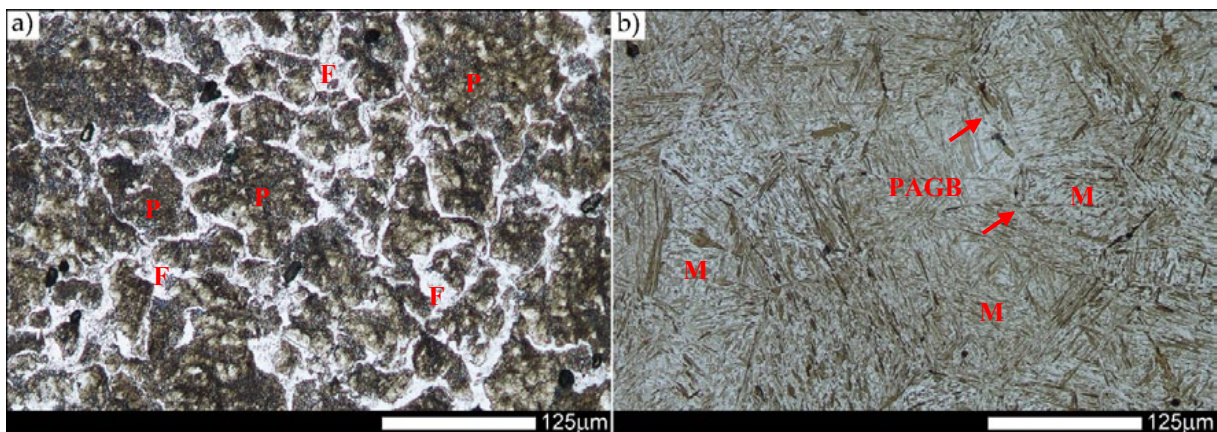


Fig. 9. Microstructures of melt 4 in different states of heat treatment: a) after full annealing; b) after quenching. Etched state, light microscopy. F – ferrite, P – perlite, M – martensite, PAGB – prior austenite grain boundary marked with arrows

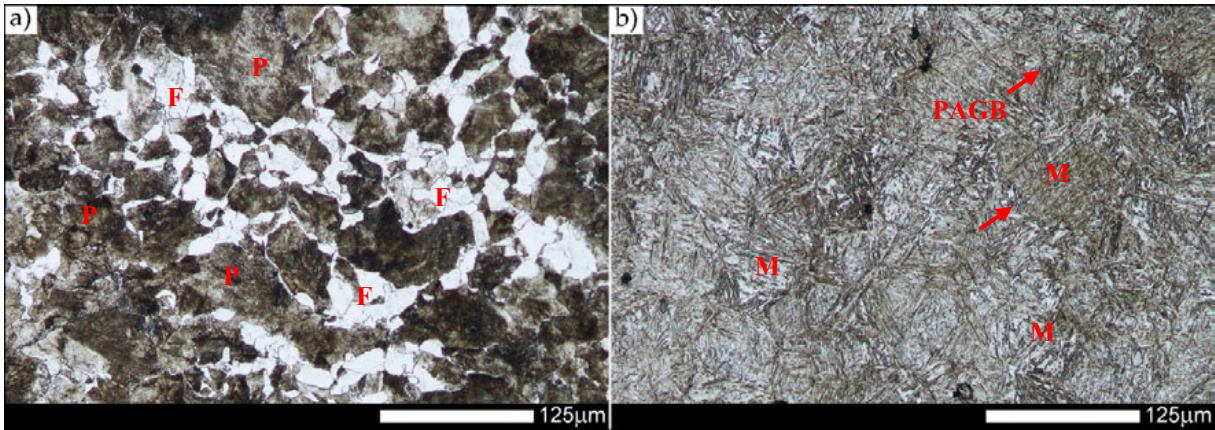


Fig. 10. Microstructures of melt 5 in different states of heat treatment: a) after full annealing; b) after quenching. Etched state, light microscopy. F – ferrite, P – perlite, M – martensite, PAGB – prior austenite grain boundary marked with arrows

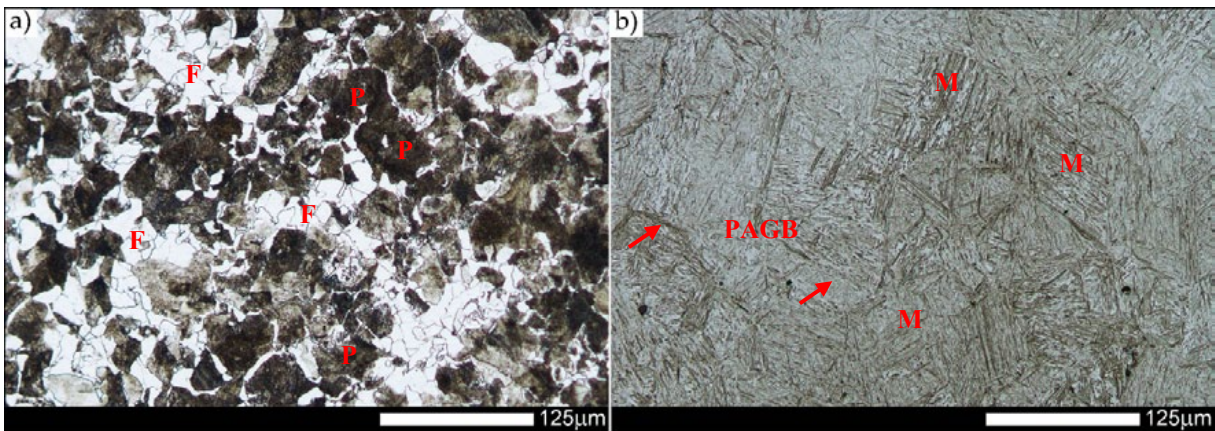


Fig. 11. Microstructures of melt 6 in different states of heat treatment: a) after full annealing; b) after quenching. Etched state, light microscopy. F – ferrite, P – perlite, M – martensite, PAGB – prior austenite grain boundary marked with arrows

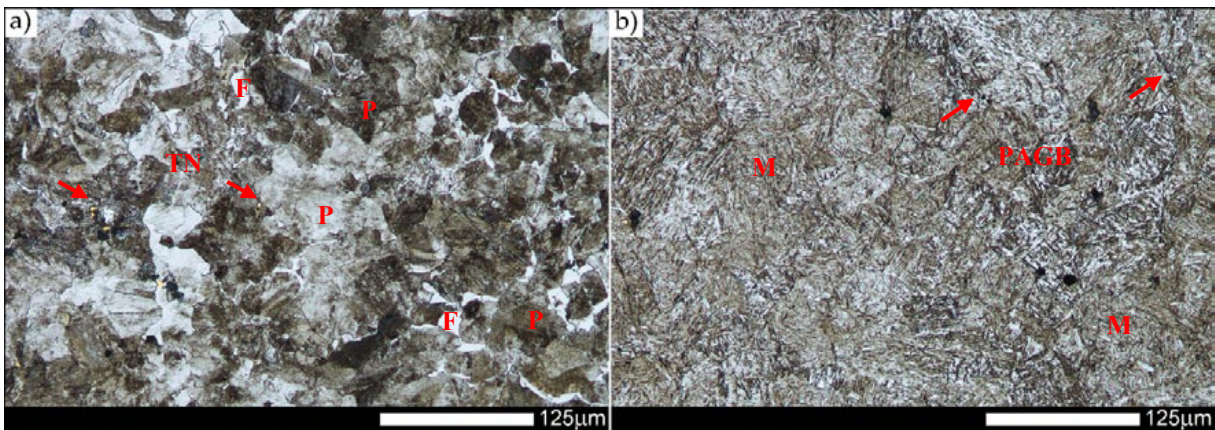


Fig. 12. Microstructures of melt 7 in different states of heat treatment: a) after full annealing; b) after quenching. Etched state, light microscopy. F – ferrite, P – perlite, M – martensite, PAGB – prior austenite grain boundary marked with arrows, TN-titanium nitrides marked with arrows

The martensite in the structure of melt 3 was clearly finer than in alloys 1 and 2, but it still showed coarseness (Fig. 8b). The hardness of the structure was higher than in cast steels 1 and 2, and was 614 HBW (Fig. 14). In the case of melt 4, the martensite was coarser, and its morphology was more acicular than lath (Fig. 9b). Between the needles, residual austenite was

clearly visible. The structure's hardness was 579 HBW (Fig. 14). Despite the presence of vanadium, the structure of melt 5 was similar to that of melt 3, while the structure of melt 6 was similar to that of melt 4. The hardness of melts 5 and 6 was similar, the highest of all analysed melts, and amounted to 622 and 621 HBW, respectively (Fig. 14). However, among the analysed cast

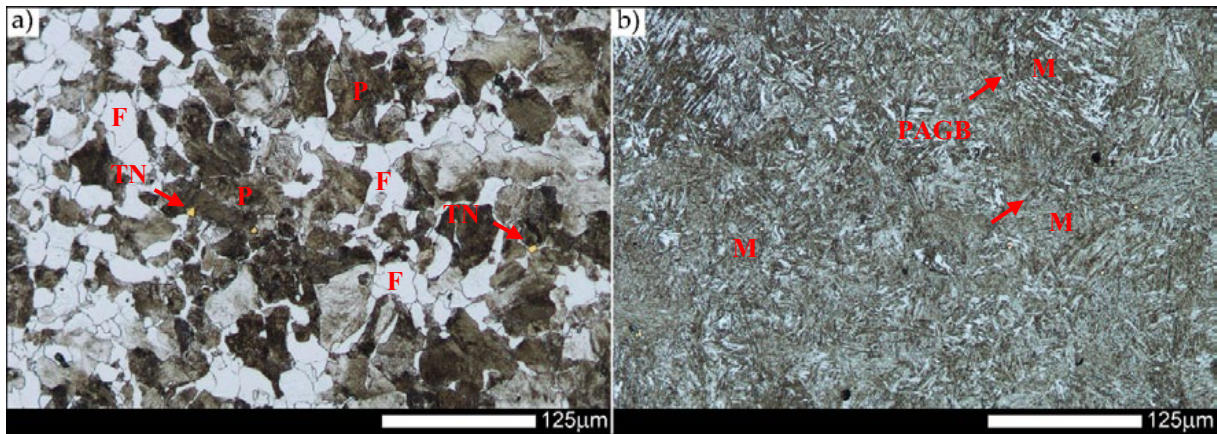


Fig. 13. Microstructures of melt 8 in different states of heat treatment: a) after full annealing; b) after quenching. Etched state, light microscopy. F – ferrite, P – perlite, M – martensite, PAGB – prior austenite grain boundary marked with arrows, TN-titanium nitrides marked with arrows

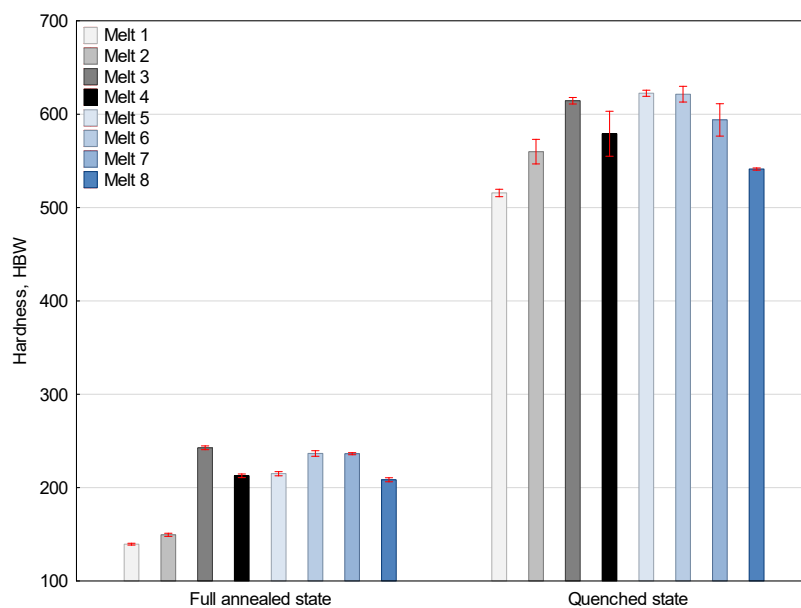


Fig. 14. Hardness of the analysed melts after full annealing and quenching

steels, it was melts 7 and 8 that showed the highest fine-grained structure, despite the high austenitizing temperature (Figs. 12b and 13b). However, the hardness of these melts was lower than that of 5 and 6, and amounted to 594 and 541 HBW, respectively (Fig. 14).

4. Conclusions

1) Boron caused a small increase in the allotropic transformation temperature in the melts without any other alloy additions. The presence of chromium practically eliminated any influence of boron on the transformation temperatures, while the presence of chromium and alloy micro-additions, such as vanadium and titanium, led to a decrease in all the phase transformation temperatures. The next stage of the research will be the development of TTT diagrams in order to illustrate the exact influence of boron on the ongoing phase transformations.

2) After full annealing, the addition of boron without any other alloy additions resulted in a clearly coarse-grained structure. In the presence of chromium, vanadium, and titanium, boron limited higher ferrite participation. Moreover, the presence of these alloy additions effectively limited the influence of boron on grain growth.

3) After quenching, the martensitic structures of melts 1 and 2 were characterised by a thick needle-shaped martensite with untransformed austenite. In melt 2, it was possible to observe acicular ferrite against its background. The structure of the melts containing chromium and vanadium were more fine-grained. In the case of melts 4 and 6, which did not contain boron, the martensite adopted a needle-like morphology. On the other hand, the finest structure was found in the melts with titanium, irrespective of whether they contained boron micro-additives. Following quenching, the hardness of the melts containing boron (except for melts 1 and 2) was higher than in the case of the melts without this element.

REFERENCES

- [1] P.L. Jain, Principles of Foundry Technology, Tata McGraw-Hill Publishing Company Limited, New Delhi (2003).
- [2] B. Kalandyk, Solidification of Metals and Alloys **31**, 83-88 (1997).
- [3] B. Kalandyk, H. Matysiak, J. Głownia, Rev. Adv. Mater. **8**, 44-48 (2004).
- [4] T.N. Baker, Y. Li, J.A. Wilson, A.J. Craven, DN. Crowther, Mater. Sci. Technol. **20** (6), 720-730 (2004).
- [5] H. Fu, Q. Xiao, J. Kuang, Z. Jiang, J. Xing, Mater. Sci. Eng. A **466** (1-2), 160-165 (2007).
- [6] P. Maitrepierre, D. Thivellier, J. Rofes-Vernis, Microstructure and Hardenability of Low-Alloy Boron-Containing Steel, in: V.D. Doane (Ed.), Hardenability Concepts with Application to Steels, AIME 34 (1977).
- [7] W.T. Llewellyn, W.T. Cook, Met. Technol. **4** (1), 265-278 (1977).
- [8] B. Białobrzaska, R. Jasiński, Ł. Konat, Ł. Szczepański Metals **11** (1), 162-180 (2021).
- [9] B. Białobrzaska, W. Dudziński, Arch. Metall. Mater. **60** (3A), 1649-1655 (2015).
- [10] B. Białobrzaska, R. Dziurka, A. Żak, P. Bała, Arch. Civ. Mech. Eng. **18** (2), 413-429 (2018).
- [11] K. Pawlak, B. Białobrzaska, Ł. Konat, Arch. Civ. Mech. Eng. **16** (4), 913-926 (2016).
- [12] B. Białobrzaska, Ł. Konat, R. Jasiński, Metals **7** (1), 26-45 (2017).
- [13] B. Białobrzaska, P. Kostencki, Wear **328**, 149-159 (2015).
- [14] Ł. Konat, J. Napiórkowski, B. Białobrzaska, Tribologia **273** (3), 67-75 (2017).
- [15] M. Szala, M. Szafran, W. Macek, S.V. Marchenko, T. Hejwowski, Adv. Sci. Technol. Res. J. **13** (4), 151-161 (2019).
- [16] J. Napiórkowski, Ł. Konat, K. Ligier, Tribologia **269** (5), 105-119 (2016).
- [17] B. Białobrzaska, Ł. Konat, Tribologia **272** (2), 7-16 (2017).
- [18] J. Napiórkowski, Ł. Konat, M. Pietruszewska, Tribologia **280** (4), 63-69 (2018).
- [19] J. Napiórkowski, M. Lemecha, Ł. Konat Tribologia **273**, 111-117 (2017).
- [20] Ł. Konat, J. Napiórkowski, K. Kołakowski, Tribologia **268** (4), 101-114 (2016).
- [21] Ł. Konat, Materials **14** (16), 4541-4580 (2021).
- [22] Ł. Konat, M. Zemlik, R. Jasinski, D. Grygier, Materials **14** (11), 2850-2894 (2021).
- [23] Ł. Konat, Materials **9** (19), 915-936 (2019).
- [24] Ł. Konat, B. Białobrzaska, P. Białek, Metals **7** (9) 349-367 (2017).
- [25] B. Białobrzaska, Ł. Konat, Tribol. Trans. **65** (2) 358-374 (2022).
- [26] K. Maruszczuk, C. Klimaszewska, J. Kolan, Technol. Exploit. Mech. Eng. **1** (1-2), 59-79 (2015).
- [27] W. Bao, L. Xing, J. Qiu, Adv. Mat. Res. **183-185**, 1918-1922 (2011).
- [28] B. Białobrzaska, Ironmak. Steelmak **48** (6), 649-676 (2021).
- [29] B. Białobrzaska, Metals **11** (4), 589-609 (2021).
- [30] H. Berns, W. Theiwen, Ferrous Materials, Springer Science & Business Media, Berlin (2008).
- [31] M. Durand-Charre, Microstructure of Steels and Cast Irons. Springer Science & Business Media, Berlin (2013).
- [32] D.A. Mortimer, M.G. Nicholas, Met. Sci. J. **10** (9), 326-332 (1976).
- [33] X.L. He, Acta Metall **37**, 147-161 (1989).
- [34] K. Seto, D. Larson, P. Warren, G.D. Smith, Scr. Mater. **40**, 1029-1034 (1999).
- [35] O.M. Akselsen, O. Grong, P.E. Kvaale, Metall. Trans. A **17A**, 1529-1536 (1986).
- [36] K.J. Irvine, F.B. Pickering, W.C. Heselwood, J. Iron Steel Inst. Jpn. **186**, 54-67 (1957).
- [37] H.E. Boyer, Atlas of Isothermal Transformation and Cooling Transformation Diagram, ASM, Michigan (1977).
- [38] O.G. Kasatkin, B.B. Vinokur, V.L. Pilyushenko, Met. Sci. Heat Treat. **26** (1-2), 27-31 (1984).